



**High Efficiency c-Silicon Solar Cells Based on  
Micro-nanoscale Structure**

**by Fred Semendy, Priyalal Wijewarnasuriya, and Nibir K. Dhar**

**ARL-TR-5576**

**June 2011**

## **NOTICES**

### **Disclaimers**

The findings in this report are not to be construed as an official Department of the Army position unless so designated by other authorized documents.

Citation of manufacturer's or trade names does not constitute an official endorsement or approval of the use thereof.

Destroy this report when it is no longer needed. Do not return it to the originator.

# **Army Research Laboratory**

Adelphi, MD 20783-1197

---

---

**ARL-TR-5576**

**June 2011**

---

---

## **High Efficiency c-Silicon Solar Cells Based on Micro-nanoscale Structure**

**Fred Semendy and Priyalal Wijewarnasuriya**  
**Sensors and Electron Devices Directorate, ARL**

**Nibir K. Dhar**  
**DARPA Microsystems Technology Office (MTO)**  
**3701 North Fairfax Drive, Arlington, VA 22203-1714**

## REPORT DOCUMENTATION PAGE

*Form Approved*  
OMB No. 0704-0188

Public reporting burden for this collection of information is estimated to average 1 hour per response, including the time for reviewing instructions, searching existing data sources, gathering and maintaining the data needed, and completing and reviewing the collection information. Send comments regarding this burden estimate or any other aspect of this collection of information, including suggestions for reducing the burden, to Department of Defense, Washington Headquarters Services, Directorate for Information Operations and Reports (0704-0188), 1215 Jefferson Davis Highway, Suite 1204, Arlington, VA 22202-4302. Respondents should be aware that notwithstanding any other provision of law, no person shall be subject to any penalty for failing to comply with a collection of information if it does not display a currently valid OMB control number.

**PLEASE DO NOT RETURN YOUR FORM TO THE ABOVE ADDRESS.**

<b>1. REPORT DATE (DD-MM-YYYY)</b> June 2011		<b>2. REPORT TYPE</b> Final		<b>3. DATES COVERED (From - To)</b>	
<b>4. TITLE AND SUBTITLE</b> High Efficiency c-Silicon Solar Cells Based on Micro-nanoscale Structure				<b>5a. CONTRACT NUMBER</b>	
				<b>5b. GRANT NUMBER</b>	
				<b>5c. PROGRAM ELEMENT NUMBER</b>	
<b>6. AUTHOR(S)</b> Fred Semendy, Priyalal Wijewarnasuriya, and Nibir K. Dhar*				<b>5d. PROJECT NUMBER</b>	
				<b>5e. TASK NUMBER</b>	
				<b>5f. WORK UNIT NUMBER</b>	
<b>7. PERFORMING ORGANIZATION NAME(S) AND ADDRESS(ES)</b> U.S. Army Research Laboratory ATTN: RDRL-SEE-I 2800 Powder Mill Road Adelphi, MD 20783-1197				<b>8. PERFORMING ORGANIZATION REPORT NUMBER</b>  ARL-TR-5576	
<b>9. SPONSORING/MONITORING AGENCY NAME(S) AND ADDRESS(ES)</b>				<b>10. SPONSOR/MONITOR'S ACRONYM(S)</b>	
				<b>11. SPONSOR/MONITOR'S REPORT NUMBER(S)</b>	
<b>12. DISTRIBUTION/AVAILABILITY STATEMENT</b> Approved for public release; distribution unlimited.					
<b>13. SUPPLEMENTARY NOTES</b> *DARPA Microsystems Technology Office (MTO), 3701 North Fairfax Drive, Arlington, VA 22203-1714					
<b>14. ABSTRACT</b> This report describes our aim to develop high-efficiency crystalline silicon (c-Si) solar cells with increased power conversion efficiency (>30%) in order to reduce solar array mass, stowed volume, and cost. Our approach is based upon increasing the electrical junction area per unit volume using microblock design and fabrication. Current thin-film and c-Si solar cells have a limited conversion efficiency of 10–20% and cost \$3–\$5/W-peak and state-of-the-art crystalline multijunction solar cells have a ~30% efficiency and cost \$30–\$40/W-peak. Increasing the conversion efficiency to >30% enables a reduction in cost to <\$1/W-peak, making the cells viable as power platforms supporting mobile wireless, laptops, residential, and commercial applications. To do this, we are moving from a two-dimensional standard flat cell to three-dimensional blocks of cells. Incorporating nanoscaled blocks in solar cell structures enhances the performances by (1) increasing the surface area-to-volume ratio; (2) bringing the junction closer to the carrier generation region, which eliminates carrier recombination; (3) increasing absorption of all incident photon flux; and (4) broadening the absorption spectrum. We have achieved a >20 times greater short-circuit current than conventional structures. We have also modeled the proposed structure to simulate key performance parameters so that they can be incorporated into the design and fabrication of the device.					
<b>15. SUBJECT TERMS</b> C-silicon, dry etching, microstructure, ICP-DRIE, solar cells					
<b>16. SECURITY CLASSIFICATION OF:</b>			<b>17. LIMITATION OF ABSTRACT</b>  UU	<b>18. NUMBER OF PAGES</b>  24	<b>19a. NAME OF RESPONSIBLE PERSON</b> Fred Semendy
<b>a. REPORT</b> Unclassified	<b>b. ABSTRACT</b> Unclassified	<b>c. THIS PAGE</b> Unclassified			<b>19b. TELEPHONE NUMBER (Include area code)</b> (301) 394-4627

---

## Contents

---

<b>List of Figures</b>	<b>iv</b>
<b>1. Introduction</b>	<b>1</b>
<b>2. Solar Cell Technology</b>	<b>3</b>
2.1 Current Solar Cell Technology.....	3
2.2 Our Approach and Goal .....	6
<b>3. Experimental</b>	<b>9</b>
<b>4. Results</b>	<b>11</b>
<b>3. Conclusion</b>	<b>13</b>
<b>4. References</b>	<b>14</b>
<b>List of Symbols, Abbreviations, and Acronyms</b>	<b>15</b>
<b>Distribution List</b>	<b>16</b>

---

## List of Figures

---

Figure 1. PV efficiency solar cells of different materials. ....	1
Figure 2. Conventional solar cell. ....	3
Figure 3. Solar radiation spectrum. ....	4
Figure 4. I-V characteristics of a solar cell. ....	5
Figure 5. (a) A conventional solar cell and (b) the proposed solar cell in this study. ....	7
Figure 6. Schematics showing the various pillar structures used in simulation. ....	8
Figure 7. Conversion efficiency comparison as parameter of pillar inclinations with structure 1: $x=D/2$ , structure 2: $x=D/4$ , and structure 3: $x=D/16$ . ....	8
Figure 8. Mask design: (a) pillar size and (b) for a 4-in Si wafer. ....	9
Figure 9. Mask design: (a) 1-cm die and (b) micro-pillars. ....	9
Figure 10. SIMS analysis of the $n^+$ Si after phosphorus implantation. ....	10
Figure 11. Fabrication process flow. ....	10
Figure 12. Thickness calculation of thermally grown $SiO_2$ . ....	11
Figure 13. Dry etch of c-Si and variations in etch profile by changing the amount of $O_2$ .....	12
Figure 14. Preliminary I-V results of fabricated solar cells under a 20-W white lamp light and room light illumination. The lamp was at a vertical distance of 18 in away from the target cells. ....	12

# 1. Introduction

In the current energy crisis, the search for a viable alternative to hydrocarbons has taken many paths: nuclear, wind, solar, etc. Solar cells provide an attractive form of limitless alternative energy. The placement of solar cells can be unobtrusive and provide not only a source of thermal energy, but electricity. However, the development and implementation of effective photovoltaic (PV) cells is hindered by two primary components: cost and efficiency. Research into cheaper and more efficient solar cells has been underway for several decades, from the development of thin-film solar cells with efficiencies greater than 10% in the 1970s to the most recent developments in new PV materials achieving greater than 24% efficiency, as shown in figure 1.

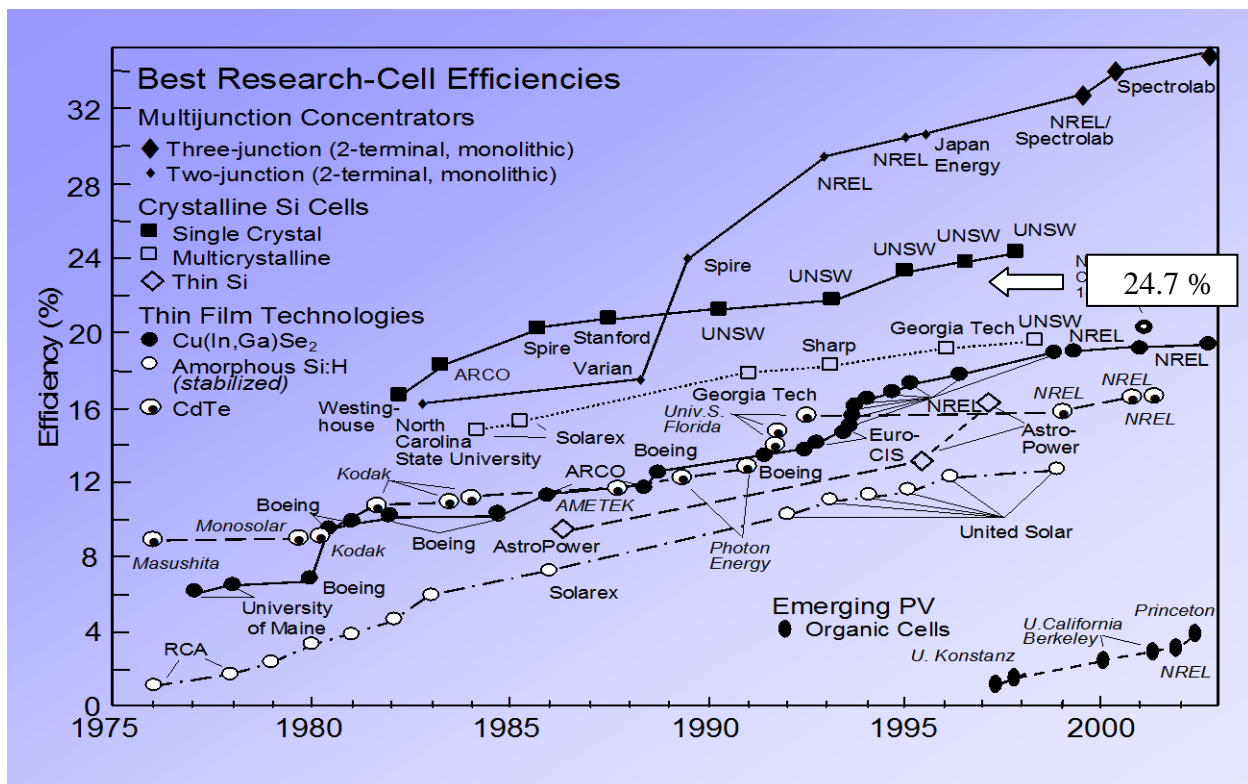


Figure 1. PV efficiency solar cells of different materials.

In general solar energy and its many applications are not widely accepted compared to conventional electrical energy solutions. The main reason for the low acceptance of solar energy is the high manufacturing costs involved. Especially in Japan and Germany, many efforts have been made to reduce manufacturing costs and expand the usability of solar energy in numerous industrial, residential, and commercial applications. In the United States, research and development (R&D) and applications are far behind other developed countries like Japan and Germany. In order to cope with the current energy crisis, it is highly desirable to build solar

energy infrastructures inside the United States alongside other energy solutions so that the United States can leapfrog other countries in the field of solar energy (1, 2).

Crystalline silicon (c-Si) and thin films (with multijunction approaches) are two major pathways to achieving solar energy goals. Each of these consists of multiple options (e.g., c-Si approaches include Si wafer and several types of sheet Si). This multiple-path characteristic makes solar cell technology robust and offers high potential for future advances in both performance improvement and cost reduction. For more demanding applications such as residential, industrial, and even, commercial solar generation systems, either polycrystalline or single-crystalline Si is the best choice due to stringent requirements for better reliability and higher efficiency than applications in consumer electronics. c-Si has a well-established technology base and the c-Si industry supplies nearly 90% of solar cell demands. c-Si will continue to dominate the market for at least five years. The technical progress will evolve, but advances will be integrated quickly into the marketplace. This will help to build the infrastructure required for continued rapid growth of solar cell technology. Cell conversion efficiencies for current c-Si approaches vary from 12% to 17% (3). Module efficiencies tend to be 0.5% to 2% lower, based on total area. However, due to the high cost of solar energy solutions (\$3 to \$5/W-peak) compared to other conventional electrical energy solutions, this Si-based solar cell is not yet widely accepted as an alternative to energy solution. As many concerns associated with a steep increase in the amount of the worldwide energy consumption are raised, further developments in c-Si solar cell technology for industrial systems applications are required and have been a primary focus.

Other leading candidates for very low-cost solar cell solutions are the following thin-film materials: (1) amorphous Si (a-Si) (4), cadmium telluride (CdTe) (5), and copper indium diselenide (CIS) (6), which are the most mature thin-film technologies; and (2) thin-film Si, which may encompass both c-Si and/or a-Si. The key metrics of thin-film progress are the same as those for any PV module technology—efficiency at the commercial module level, manufacturing cost, and outdoor module reliability. Many challenges must be overcome before these factors can be optimized. For thin films, the monolithic process blurs the distinction between cells and modules. However, commercial module efficiencies vary between 5% and 11%. The cost of these thin-film solar cells (\$3 to \$5/W-peak) is almost same as that of c-Si. However, due to the toxic natures of these materials and concerns for the environment, thin-film-based solar cells are not widely accepted.

To achieve a higher conversion efficiency (20% and higher), conventional multijunction combinations of III-V semiconductors are usually used (7, 8). The materials and manufacturing cost of the multijunction solar cell costs more than 10 times that of Si solar cells. It is highly desirable to have an alternative solution of a solar cell made of Si, which could offer a higher efficiency (20% and higher) and have a comparable or lower cost than today's Si solar cell.

We propose a solar cell structure that would be environmentally friendly, highly efficient, and cost effective. In this report, we provide an overview of a high-efficiency Si solar cell based on

micro-nanostructures, which can be fabricated using standard Si integrated circuit (IC) technology and is amenable to mass-scale production. Details of simulation and fabrication technology are also provided. We believe the proposed high-efficiency Si solar cell could eliminate the energy crisis and greatly benefit the United States in many ways.

---

## 2. Solar Cell Technology

---

Before providing the technical approach for significantly increasing the conversion efficiency (>20%) of c-Si solar cells using less Si material (0.6 g/W, final target), we present an overview of current solar cell solutions and their limitations with regard to making high-efficiency solar cells.

### 2.1 Current Solar Cell Technology

Solar cell structures have been studied extensively over the last decade for various applications. Figure 2 is a conventional solar cell comprising a thick p-type semiconductor layer and a thin n-type semiconductor layer formed on an electrically conductive substrate.

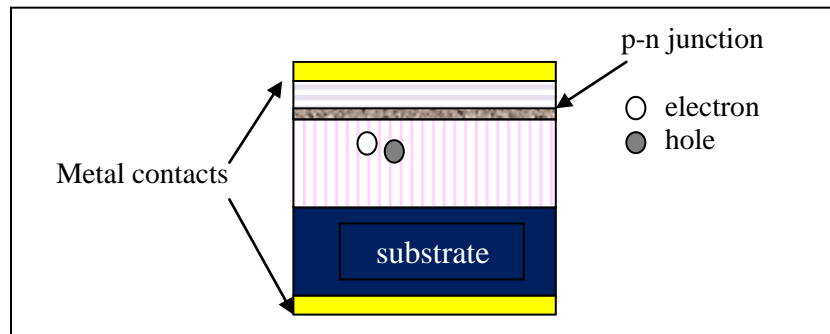


Figure 2. Conventional solar cell.

A p-n-junction is formed at the interface between the p- and n-type semiconductor layers. Incident sunlight entering in the cell generates electron-hole pairs after being absorbed by the p- and n-type semiconductor layers. The incident light generates electrons and holes in the region near the p-n-junction and far from the p-n junction. The photogenerated electrons diffusing toward the p-n junction and entering the p-n junction region contribute to the PV effect. The two key factors that substantially impact the conversion efficiency of solar cell are photocarrier generation efficiency (PCGE) and photocarrier collection efficiency (PCCE). For monochromatic light, a PCGE of ~100% can be achieved by simply making the p-type layer thicker. However, electrons generated at the region far from the p-n junction cannot be collected efficiently due to many adverse recombination processes. These processes prevent photogenerated carriers from diffusing into the p-n junction, thus the basic structure of current PV cells has its own limitation on increasing the conversion efficiency.

The light intensity  $p$  at certain depth  $x$  can be expressed by  $p(x)=Poexp(-\alpha x)$ , where  $Po$  is the peak intensity at the surface and  $\alpha$  is the absorption co-efficient of the semiconductor into which light enters. The light intensity behavior inside a bulk semiconductor is approximately exponential in behavior. Carriers (not shown in figure 2) generated due to light flux absorbed by the p-n junction are only drifted by the junction field and can be collected efficiently. Conversely, carriers generated due to absorption of light flux by the semiconductor region are diffused in all directions. Only those which are generated closer (a separation distance equal to or less than the diffusion-length of the semiconductor) to the p-n junction can be collected. Carriers that are generated far away (a separation distance longer than the diffusion-length of the semiconductor) from the p-n junction are recombined and lost. The light flux is usually lost either by escaping or being absorbed by the substrate. For these reasons, it is difficult to increase the conversion efficiency of the cell if the standard structure is used. Apart from these, one has to consider the bulk recombination process, which reduces the minority carrier lifetime. To alleviate this, we need defect-free materials. In addition, the nature of the surface plays an important role. High reflection at the illuminated surface can be avoided by antireflection coating and other light-trapping effects. Because of the bandgap limitations, long wavelength light escapes in Si, which can be avoided by having multiple passes, optimizing the reflection from front to back and front surfaces, and optimizing the substrate thickness.

The solar spectrum is shown in figure 3. The spectrum, as seen from a satellite, is referred to as the AM0 spectrum (where AM stands for air mass) and closely fits the spectrum of a black body at 5800 K. The total power density is 1353 W/m<sup>2</sup>.

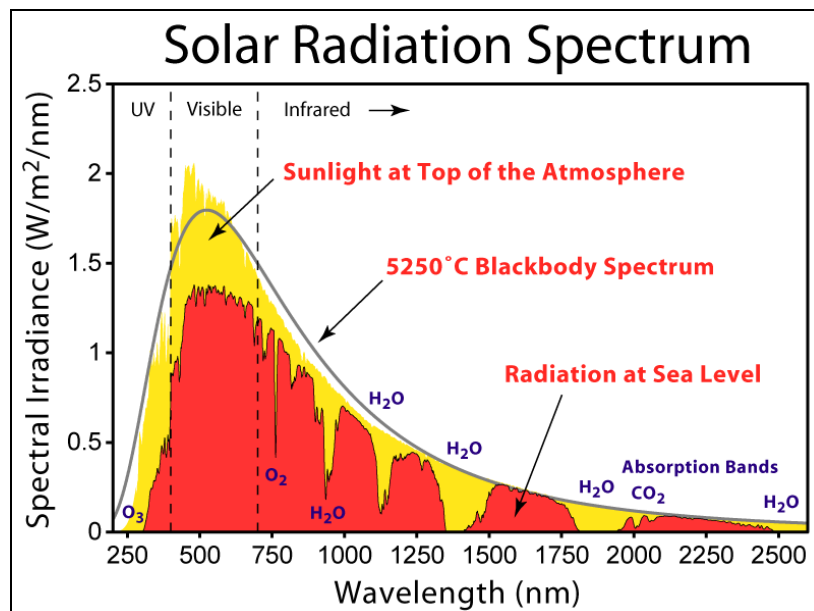


Figure 3. Solar radiation spectrum.

The solar spectrum, as observed on Earth, is modified due to absorption in the atmosphere. For AM1 (normal incidence), the power density is reduced to  $925 \text{ W/cm}^2$ ; whereas, for AM1.5 ( $45^\circ$  above the horizon), the power density is  $844 \text{ W/m}^2$ . The irregularities in the spectrum are due to absorption at specific photon energies. Figure 4 gives the current-voltage (I-V) graph for a solar cell.

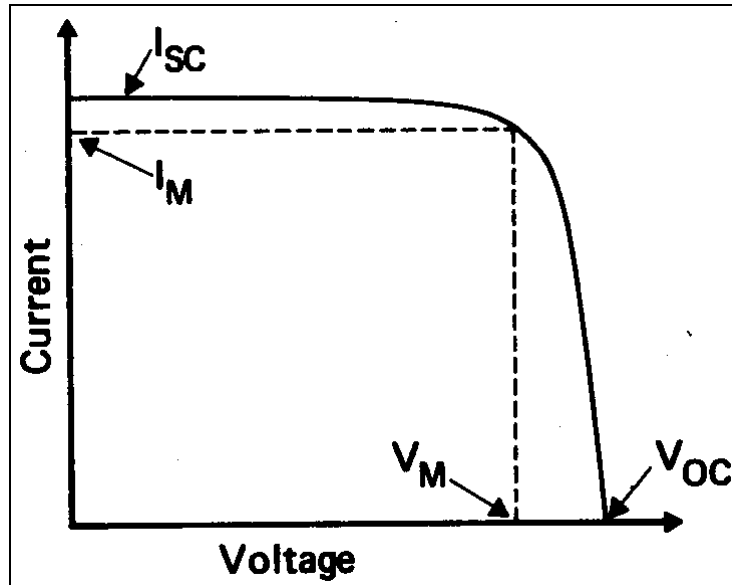


Figure 4. I-V characteristics of a solar cell.

The important parameters for calculating power conversion are the following:

- The short-circuit current ( $I_{SC}$ ) is the point at which the I-V curve crosses the  $x$ -axis at  $0 \text{ V}$ . When a solar cell is operated at short circuit (that is, when a low-resistance connection is established by accident or intention between two points in an electric circuit so the current tends to flow through the area of low resistance bypassing the rest of the circuit),  $V = 0$  and the current ( $I$ ) through the terminals is defined as the short-circuit current.
- The open-circuit voltage ( $V_{OC}$ ) is the voltage at which there is zero current flow. When a cell is operated at open circuit (that is, an incomplete electrical circuit in which no current flows,  $I = 0$ ), the voltage across the output terminals is defined as the open-circuit voltage.
- The maximum power output ( $P_{MAX}$ ) is the voltage and current points where the cell is generating its maximum power. The  $P_{MAX}$  point on an I-V curve is often referred to as the maximum power point (MPP).
- The current at maximum power ( $I_m$ ) is the cell's current level at  $P_{MAX}$ .
- The voltage at maximum power ( $V_m$ ) is the cell's voltage level at  $P_{MAX}$ .
- Fill factor (FF) is  $P_{MAX}$  divided by  $V_{OC}$  multiplied by  $I_{SC}$ . FF is a popular measurement because it indicates the cell's efficiency under a specific spectrum and intensity of light. In

essence, it calculates the percentage of performance of the real cell versus an ideal cell with no internal losses. Thus, by using the diode equation and  $V_{OC}$ , and manipulating a number of equations, one can arrive at the power conversion efficiency,

$$\eta = \frac{V_m I_m}{P_{in}}, \quad (1)$$

which can be further modified by substituting for  $I_m$

$$\eta = \frac{V_m q A_a \int \phi(\lambda) QE(\lambda) d\lambda}{A_t \int \phi(\lambda) \frac{hc}{\lambda} d\lambda}, \quad (2)$$

where  $A_a$  is the active area and  $A_t$  is the total area. Thus, by increasing the junction area, one can maximize the power conversion efficiency. Therefore, our goal is to increase the volume-to-surface area ratio using microblock design masks. Using this technique, large junction areas can be made using microstructural fabrication, in which the junction is closer to the carrier generation region, thus reducing carrier recombination. The design is easy to implement and is independent of the material system.

## 2.2 Our Approach and Goal

The proposed solar cell structure consists of a number of micro-nanoscaled blocks (micro-nanorods/wires) around and on which the p-n junction is formed, thereby increasing surface (junction) area, as shown in figure 5. The p-n junction is formed very close to the region where the carriers are generated; thus, all photogenerated carriers can be collected before recombination. Furthermore, incorporation of these nanoscaled blocks into the solar cell structure can create quantum confinement and intermediate states within the bandgap to harvest photons with energy less than that of the bandgap of the host material. In this way, nanoscaled block structures in the proposed solar cells can be optimized to absorb a large portion of the solar spectrum. The front-side contact is transparent so that light can pass through the semiconductor, and the back-side contact is formed on the substrate. Differences in the proposed solar cell over conventional solar cells include a larger junction area due to use of nano (or micro) structures and the creation of a junction closer to the carrier generation region, which eliminates carrier recombination. In addition, most of the incident photons flux is absorbed due to the angular nature of the microstructure. Furthermore, there is less usage of Si, which, in turn, makes the device more cost effective, enabling it to be used as the universal structure for significantly high-efficiency solar cells. Precise control of the nano (or micro) cylindrical blocks' (a.k.a., pillars) length, density per unit area, reliability, and mechanical robustness will be ensured. The proposed unique and novel structure approaches will open doors to the incorporation of nano/microscaled cylindrical blocks for designing significantly high-conversion-efficiency solar cells.

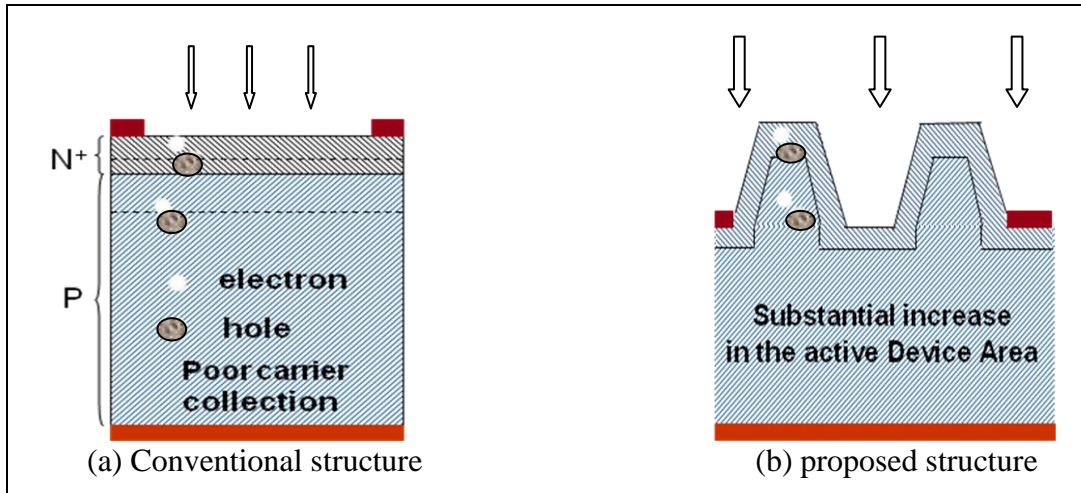


Figure 5. (a) A conventional solar cell and (b) the proposed solar cell in this study.

The proposed solar cell can be made from any kind of system material. For example, the substrate material can be any semiconductor, such as Si, gallium arsenide (GaAs), indium phosphide (InP), etc., glass, metal, or polymer. If the substrate is a semiconductor such as Si, micro-nanopillars can be formed using the etching approach, and if the substrate base material is InP, similar micro-nanopillars can also be made on the substrate. The proposed structure can also be fashioned from polymer to make the solar cells flexible. In this case, nanorods can be incorporated into the polymer materials to make a flexible solar cell using the proposed structure. We propose to fabricate the solar cell based on micro-nanocylindrical blocks, having a high conversion efficiency and high Si intensity.

We have carried out the simulation and also fabricated test structures on the proposed solar cell incorporating cylindrical structures. Initial experimental results demonstrated that the proposed solar cell showed significant conversion efficiency (>20 times greater compared to conventional cells). Theoretical estimated results showed that the conversion efficiency can be increased to >30% for a c-Si solar cell. Simulation and experimental results are explained in sections 3 and 4.

The proposed structure was calculated for a Si-based solar cell to see the benefits of the structure, varying the side tilting angle at fixed height of 5  $\mu\text{m}$ . Noted here that the thickness of the c-Si wafer ( $5 \times 10^{17} \text{cm}^{-3}$ ) considered in the simulation was 350  $\mu\text{m}$ , which is frequently used in solar cell fabrication. A shallow p-n junction of 0.1  $\mu\text{m}$  was considered in the simulation. A vertical trapezoidal structure was assumed to be formed using the Si wafer. In simulation, it was also assumed that the carrier movement was mainly dominated by diffusion, rather than drift, as the estimation of the depletion region due to built-in-potential was 120 nm. We used standard solar irradiance and the absorption coefficient for Si in simulation.

Figures 6 and 7 show the simulation results of conversion efficiencies at various tilting angles. Pillar structure 1 shows less angle and structure 3 shows a  $86^\circ$  angle, nanopillar (conventional), without the pillar case. Decreasing the tilting angle offers higher conversion efficiencies over 35%, which are thought to be due to (1) increasing the junction area, (2) increasing the

absorption spectra, and (3) increasing the light intensity due to the self-concentrating effect of the cylinder (pillar). More simulation and optimization are necessary to accurately access the conversion efficiency for the proposed structure.

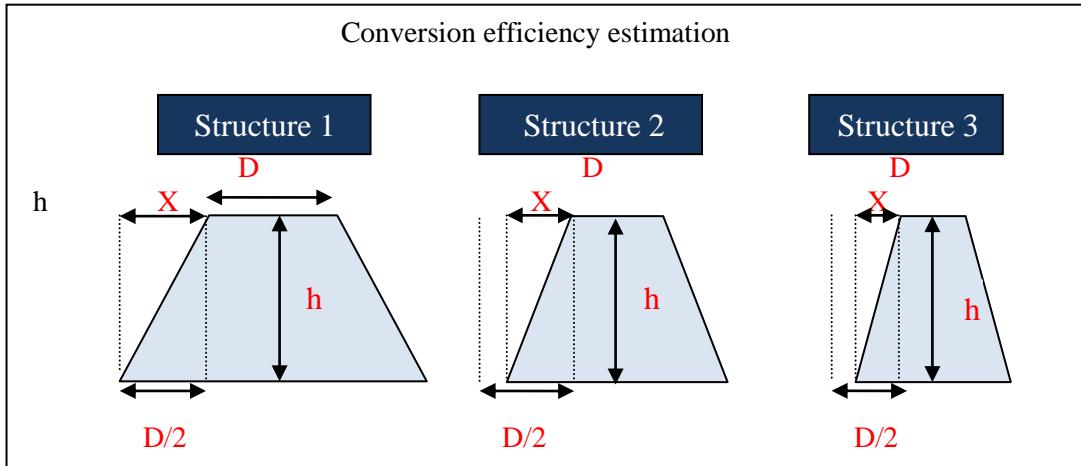


Figure 6. Schematics showing the various pillar structures used in simulation.

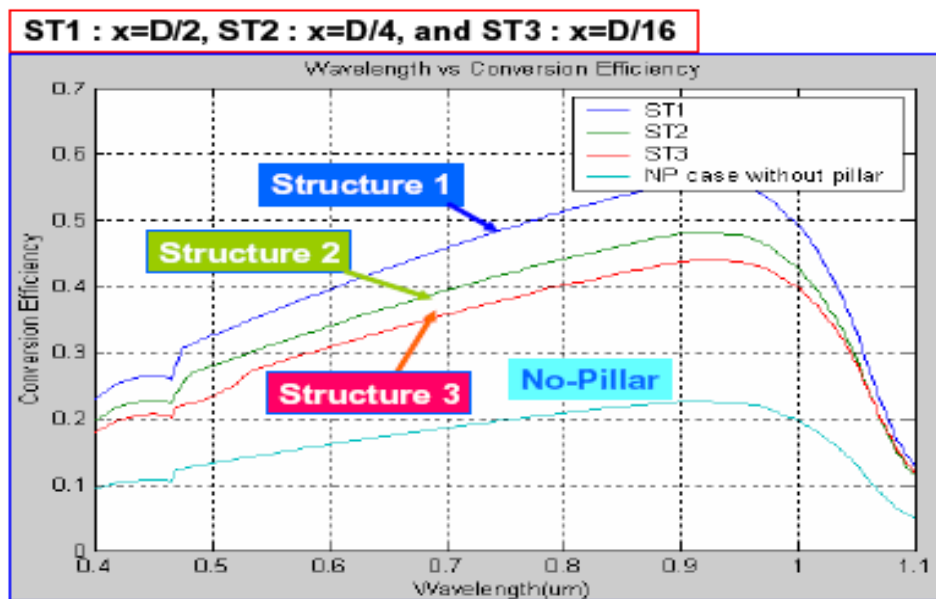


Figure 7. Conversion efficiency comparison as parameter of pillar inclinations with structure 1:  $x=D/2$ , structure 2:  $x=D/4$ , and structure 3:  $x=D/16$ .

### 3. Experimental

The proposed solar cell structure based on micro-nanopillars was fabricated using a c-Si solar cell. Figure 8 shows the mask design part of the work with (a) the pillar size in consideration and (b) for a 4-in Si wafer. Figure 9 shows (a) a 1-cm die and (b) the micro-pillar etching area showing the size of the pillar ( $2\ \mu\text{m}$ ).

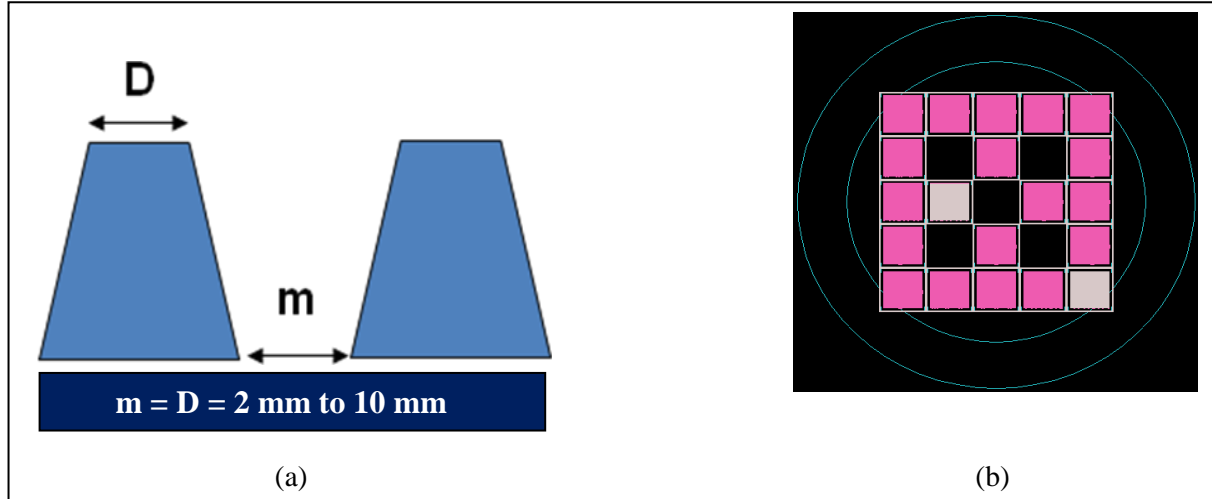


Figure 8. Mask design: (a) pillar size and (b) for a 4-in Si wafer.

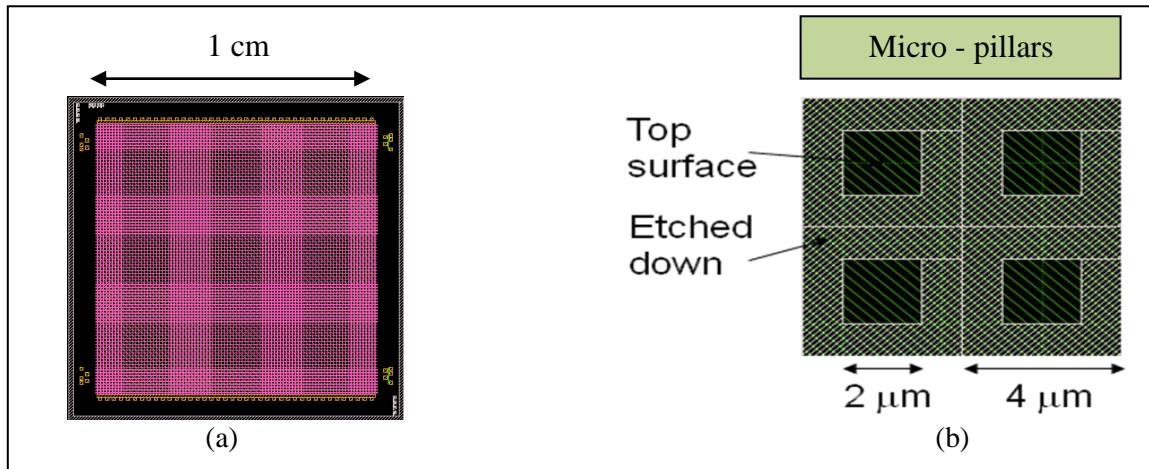


Figure 9. Mask design: (a) 1-cm die and (b) micro-pillars.

Boron-doped, 4-in crystalline Si wafers with a conductivity of  $10\ \Omega\text{cm}$  and a thickness of  $500\ \mu\text{m}$  were used for the fabrication. The wafer was p-type doped at  $\sim 10^{15}\ \text{cm}^{-3}$ . For the junction formation, phosphorus was ion implanted at an energy level of  $100\ \text{keV}$  with a dosage of  $3 \times 10^{13}\ \text{cm}^{-2}$  to enhance the layer to  $n^+$ . Secondary ion mass spectrometry (SIMS) analysis was performed to verify the doping level and the results are shown in figure 10.

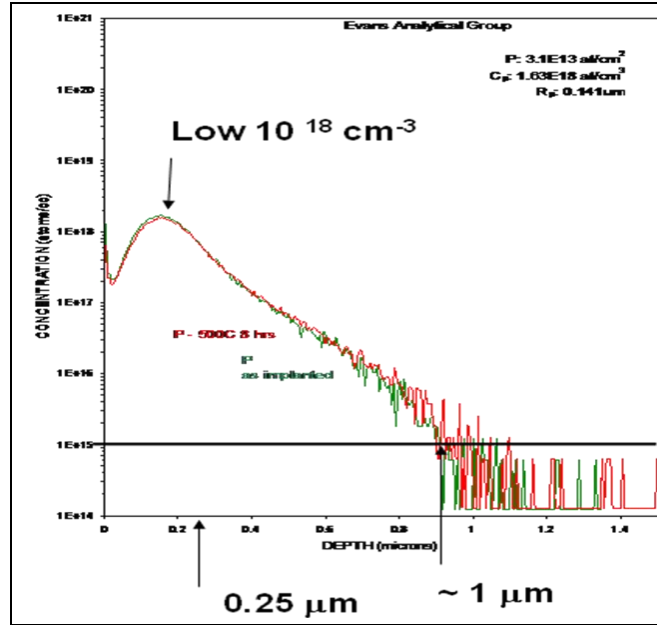


Figure 10. SIMS analysis of the n<sup>+</sup> Si after phosphorus implantation.

The fabrication process flow for the c-Si solar cell with micro-nanopillars is shown in figure 11. To form vertically arranged and well-defined microblocks in the c-Si (<100>) substrate, the standard dry-etching technique was used. After cleaning the wafer using the standard cleaning procedures, photolithographic techniques were used to define the micro-pillar structure. This was followed by etching using the inductively coupled plasma (ICP) deep reactive ion etching (DRIE) technique.

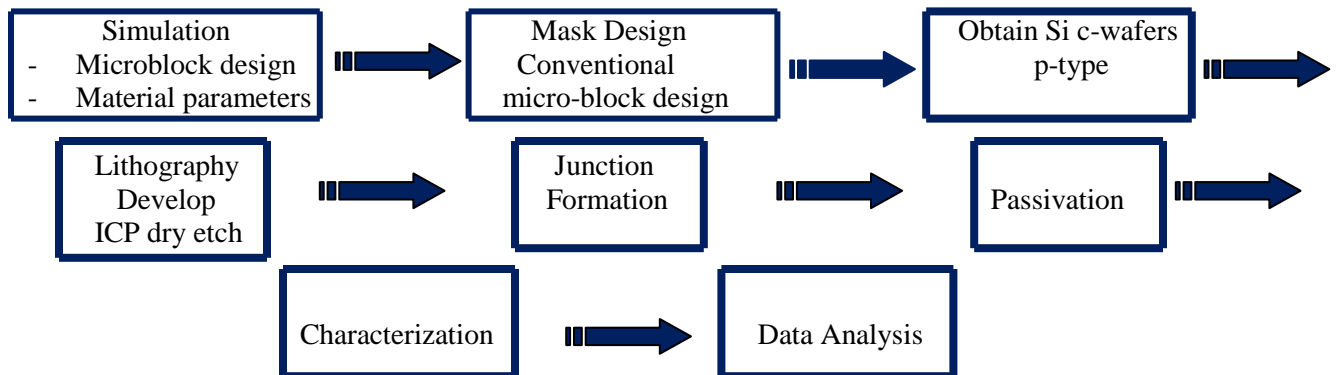


Figure 11. Fabrication process flow.

A mixed gas system of sulfur hexafluoride (SF<sub>6</sub>) and oxygen (O<sub>2</sub>) was used for the dry etching with varying pressures, gas ratios, times, and temperatures. Cleaned wafers were n<sup>+</sup> ion implanted, followed by passivation using thermal growth of silicon dioxide (SiO<sub>2</sub>). The thickness of the thermally grown SiO<sub>2</sub> is calculated as shown in figure 12.

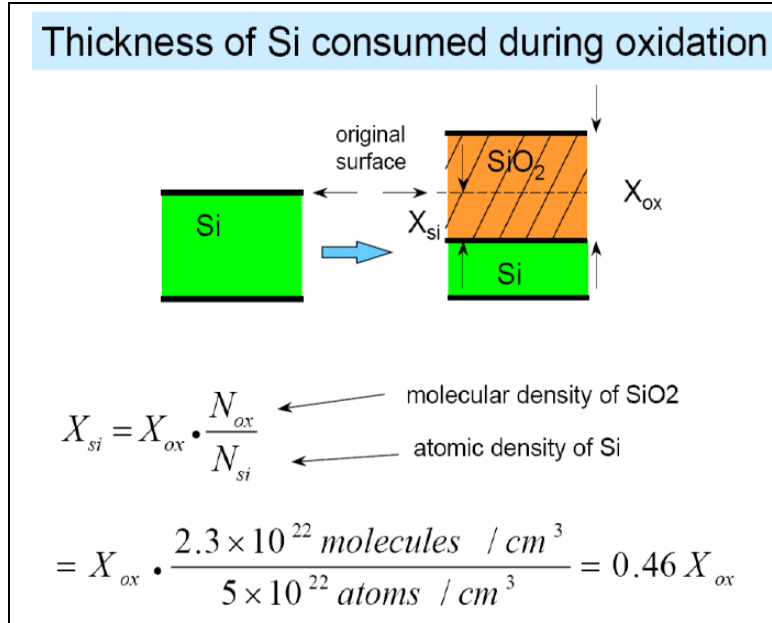


Figure 12. Thickness calculation of thermally grown SiO<sub>2</sub>.

After passivation and metallization, devices were characterized and data were analyzed.

## 4. Results

The dry-etch process to create the micro-pillars was found to be complicated and difficult to optimize. Parameters such as pressure, amount of gas, radio frequency (RF), ICP power, time, and gas ratio had to be varied to obtain the right recipe to etch down and create the micro-pillars. Figure 13 shows some of the micro-pillars obtained by ICP-DRIE process. As shown in the image, the walls are vertical in the etch process. The actual case (as shown in figure 13) demonstrates how not enough O<sub>2</sub>, the right amount of O<sub>2</sub>, and excess amount of O<sub>2</sub> can provide the best possible etch required by the modeling. In the actual experiment, along with the variations in the amount of O<sub>2</sub> used, changes in other parameters were also made to fine-tune to optimize the etch process.

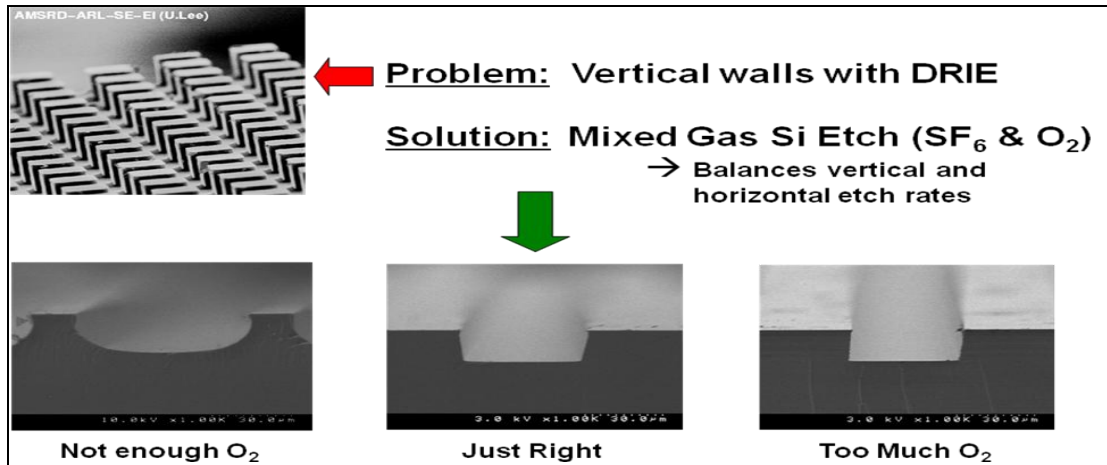


Figure 13. Dry etch of c-Si and variations in etch profile by changing the amount of  $\text{O}_2$ .

For the fabrication of the devices, we used conventional cells of  $1 \times 1 \text{ cm}^2$  from a 4-in silicon wafer. After the fabrication process, each cell was diced out and wire bonded for characterization. A 20-W white lamp light was used for the initial I-V characterization. During the measurement, the lamp was kept at a vertical height of 18 in, directly above the sample. Figure 14 shows the preliminary I-V characteristics of the solar cells and the conventional (flat, without pillar) cell.

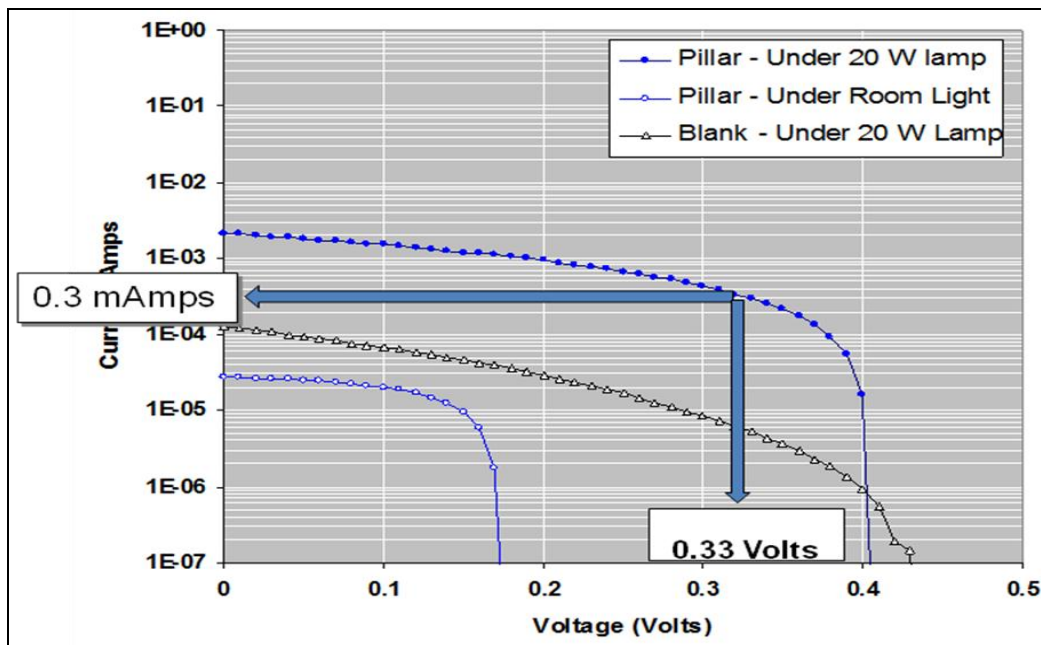


Figure 14. Preliminary I-V results of fabricated solar cells under a 20-W white lamp light and room light illumination. The lamp was at a vertical distance of 18 in away from the target cells.

Conversion power for the micro-pillar and conventional cells was found to be 200 and 20  $\mu\text{W}$ , respectively, showing a more than  $\sim 180 \mu\text{W}$  power difference. Further optimization of fabrication process and structural designs are necessary to further enhance the conversion efficiency performance. *Initial experimental results indicate that the proposed solar cell structure promises to improve the conversion efficiency using thinned substrates of any material system.* The proposed solar cell structure is expected to offer higher efficiency for all semiconductor materials as compared with the standard solar cell. Even though the final power conversion efficiency was not as expected, we intend to optimize the process by (1) dry etching specially on smaller scale pillars, (2) optimizing the lithography, (3) improving the P and  $n^+$  contacts, (4) implanting conditions for the P dopant, (5) diffusing P into silicon, (6) solving the passivation issues, and (7) exploring the possibility of boron doping in Si. These optimizing processes can be tried on c-Si as well as in thin solar cell materials.

---

### **3. Conclusion**

---

In this report, we present a high-efficiency Si solar cell that consists of micro-nanoblocks with an increased surface area-to-volume ratio and a p-n junction over the 3-D blocks for the top and bottom contacts. Simulation results indicate that (1) the absorption efficiency was increased due to self concentrating or photon trapping and (2) the absorption spectra increased in comparison with the flat device. Simulation from first principles indicates that the short-circuit current increased due to bringing the junction closer to the carrier generation sites. These phenomena increased the conversion efficiency of the Si solar cell. Experimental results of the solar cell fabricated using conventional photolithographic techniques showed that the short-circuit current of the solar cell based on the micro-nanoscale structures was 18 times greater than the standard solar cell fabricated on the same Si substrate.

In order to develop this high-efficiency solar cell, we will need to further optimize the design and iterate the parameters to accurately model the proposed solar cell, and then evaluate and demonstrate our ability to fabricate the optimized solar cell.

We believe that proposed solar cell technology will enable a high-conversion-efficiency, cost-effective solar cell technology that can be mass-produced and customized for commercial and defense systems.

---

## 4. References

---

1. The U.S. Photovoltaic Industry Roadmap. National Renewable Energy Laboratory: Golden, CO, January 2003.
2. World Energy Outlook 2001, published by the Energy Information Administration (EIA).
3. Zhao, J.; Wang, A.; Green, M.; Ferrazza, F. Novel 19.8% Efficient ‘Honeycomb’ Textured Multicrystalline and 24.4% Monocrystalline Silicon Solar Cell. *Applied Physics Letters* **1998**, *73*, 1991–1993.
4. Yamamoto, K.; Yoshimi, M.; Suzuki, T.; Tawada, Y.; Okamoto, T.; Nakajima, A. Thin Film Poly-Si Solar Cell on Glass Substrate Fabricated at Low Temperature. *Presented at MRS Spring Meeting*, San Francisco, CA, April 1998.
5. Wu, X.; Keane, J. C.; Dhere, R. G.; DeHart, C.; Duda, A.; Gessert, T. A.; Asher, S.; Levi, D. H.; Sheldon, P. 16.5%-efficient CdS/CdTe Polycrystalline Thin-film Solar Cell. *Proceedings of the 17th European Photovoltaic Solar Energy Conference*, Munich, Germany, 22–26 October 2001, 995–1000.
6. Contreras, M. A.; Egaas, B.; Ramanathan, K.; Hiltner, J.; Swartzlander, A.; Hasoon, F.; Noufi, R. Progress Toward 20% Efficiency in Cu(In,Ga)Se Polycrystalline Thin-film Solar Cell. *Progress in Photovoltaics: Research and Applications* **1999**, *7*, 311–316.
7. King, R. R.; Fetzer, C. M.; Colter, P. C.; Edmondson, K. M.; Law, D. C.; Stavrides, A. P.; Yoon, H.; Kinsey, G. S.; Cotal, H. L.; Ermer, J. H.; Sherif, R. A.; Karam, N. H. Lattice-matched Proc. of SPIE Vol. 7683 768300-13 Downloaded from SPIE Digital Library on 02 Mar 2011 to 158.12.36.175. Terms of Use: <http://spiedl.org/terms> and metamorphic GaInP/GaInAs/Ge concentrator solar cells. *Proceedings of the World Conference on Photovoltaic Energy Conversion (WCPEC-3)*, Osaka, Japan, May 2005.
8. Multijunction Solar Cell, DOE Research Report, 2004.
9. Taguchi, K. *Ch. 2, WDM Technologies: Active Optical Components*; Achyut Dutta, et Al., eds., Academic Press: San Diego, CA, 2002.

---

## List of Symbols, Abbreviations, and Acronyms

---

a-Si	amorphous SI
CdTe	cadmium telluride
c-Si	crystalline silicon
CIS	copper indium diselenide
DRIE	deep reactive ion etching
FF	fill factor
GaAs	gallium arsenide
I	current
IC	integrated circuit
ICP	inductively coupled plasma
InP	indium phosphide
I <sub>sc</sub>	short-circuit current
I-V	current-voltage
MPP	maximum power point
O <sub>2</sub>	oxygen
P <sub>MAX</sub>	maximum power output
PCCE	photocARRIER collection efficiency
PCGE	photocARRIER generation efficiency
PV	photovoltaic
R&D	research and development
RF	radio frequency
SF <sub>6</sub>	sulfur hexafluoride
SiO <sub>2</sub>	silicon dioxide
SIMS	secondary ion mass spectrometry
V <sub>oc</sub>	open-circuit voltage

NO. OF COPIES	ORGANIZATION	NO. OF COPIES	ORGANIZATION
1 ELECT	ADMNSTR DEFNS TECHL INFO CTR ATTN DTIC OCP 8725 JOHN J KINGMAN RD STE 0944 FT BELVOIR VA 22060-6218	1	US GOVERNMENT PRINT OFF DEPOSITORY RECEIVING SECTION ATTN MAIL STOP IDAD J TATE 732 NORTH CAPITOL ST NW WASHINGTON DC 20402
1	DARPA MTO ATTN N DHAR 3701 NORTH FAIRFAX DR ARLINGTON VA 22203-1714	1	GENERAL TECHNICAL SERVICES ATTN G P MEISSNER 3100 ROUTE 138 WALL NJ 07719
1 CD	OFC OF THE SECY OF DEFNS ATTN ODDRE (R&AT) THE PENTAGON WASHINGTON DC 20301-3080	1	DIRECTOR US ARMY RSRCH LAB ATTN RDRL ROE L W CLARK PO BOX 12211 RESEARCH TRIANGLE PARK NC 27709
1	US ARMY RSRCH DEV AND ENGRG CMND ARMAMENT RSRCH DEV & ENGRG CTR ARMAMENT ENGRG & TECHN LGY CTR ATTN AMSRD AAR AEF T J MATTS BLDG 305 ABERDEEN PROVING GROUND MD 21005-5001	62	U.S. ARMY RSRCH LAB ATTN IMNE ALC HRR MAIL & RECORDS MGMT ATTN RDRL CIO LL TECHL LIB ATTN RDRL CIO MT TECHL PUB ATTN RDRL SE T BOWER ATTN RDRL SE J PELLEGRINO ATTN RDRL SED E B MORGAN ATTN RDRL SED E K A JONES ATTN RDRL SED E M LITZ ATTN RDRL SED P A LELIS ATTN RDRL SEE E K ALIBERTI ATTN RDRL SEE E N GUPTA ATTN RDRL SEE E R TOBER ATTN RDRL SEE E T ALEXANDER ATTN RDRL SEE G WOOD ATTN RDRL SEE I S TRIVEDI ATTN RDRL SEE I B ZANDI ATTN RDRL SEE I D BEEKMAN ATTN RDRL SEE I F SEMENDY (5 COPIES) ATTN RDRL SEE I G BRILL ATTN RDRL SEE I J LITTLE ATTN RDRL SEE I K K CHOI ATTN RDRL SEE I K OLVER ATTN RDRL SEE I P FOLKES ATTN RDRL SEE I P TAYLOR ATTN RDRL SEE I P UPPAL ATTN RDRL SEE I S FARRELL (3 COPIES) ATTN RDRL SEE I S SVENSSON ATTN RDRL SEE I W BECK
3	CECOM NVESD ATTN AMSEL RD NV ATTN AMSEL RD NV A SCHOLTZ ATTN AMSEL RD NV D BENSON 10221 BURBECK RD STE 430 FT BELVOIR VA 22060-5806		
1	PM TIMS, PROFILER (MMS-P) AN/TMQ-52 ATTN B GRIFFIES BUILDING 563 FT MONMOUTH NJ 07703		
1	US ARMY INFO SYS ENGRG CMND ATTN AMSEL IE TD A RIVERA FT HUACHUCA AZ 85613-5300		
1	COMMANDER US ARMY RDECOM ATTN AMSRD AMR W C MCCORKLE 5400 FOWLER RD REDSTONE ARSENAL AL 35898-5000		

NO. OF  
COPIES ORGANIZATION

ATTN RDRL SEE I W SARNEY  
ATTN RDRL SEE I Y CHEN  
ATTN RDRL SEE L BLISS  
ATTN RDRL SEE M G DANG  
ATTN RDRL SEE M G GARRETT  
ATTN RDRL SEE M M REED  
ATTN RDRL SEE M  
M TAYSING-LARA  
ATTN RDRL SEE M M WRABACK  
ATTN RDRL SEE M N BAMBHA  
ATTN RDRL SEE M N DAS  
ATTN RDRL SEE M P SHEN  
ATTN RDRL SEE M W CHANG  
ATTN RDRL SEE O N FELL  
ATTN RDRL SEE O P PELLEGRINO  
ATTN RDRL SEE P GILLESPIE  
ATTN RDRL SEG N MARK  
(3 COPIES)  
ATTN RDRL SER E A DARWISH  
ATTN RDRL SER E P SHAH  
ATTN RDRL SER L A WICKENDEN  
ATTN RDRL SER L B NICHOLS  
ATTN RDRL SER L E ZAKAR  
ATTN RDRL SER L M DUBEY  
ATTN RDRL SER L M ERVIN  
ATTN RDRL SER L S KILPATRICK  
ATTN RDRL SER P AMIRTHARAJ  
ATTN RDRL SER U C FAZI  
ADELPHI MD 20783-1197

TOTAL: 75 (73 HCS, 1 CD, 1 ELECT)

INTENTIONALLY LEFT BLANK.